# Optical properties of selenium

Heikki M. Isomäki

*Electron Physics Laboratory and Department of General Sciences, Helsinki University of Technology,*
*SF-02150 Espoo 15, Finland*

The permittivity, reflectivity, absorption coefficient, and electron-energy-loss function of trigonal Se are calculated from 0 to 25 eV with the use of the self-consistent non-muffin-tin Hartree-Fock-Slater band-structure results obtained with the orthogonalized-plane-wave method. The momentum matrix elements for the Ehrenreich-Cohen permittivity tensor are rigorously calculated in the bulk of the first Brillouin zone. The calculated spectra agree closely with the experimental ones. The interpretation of all the main peaks and anisotropies in the spectra are given in terms of the transitions between the band groups. The analysis provides new insight into the origin of the main optical features of Se above $\sim 5$ eV (i.e., above the energy range of the first main peak in the optical spectra). The results are also used to interpret the imaginary part of the permittivity of amorphous Se. The effect of the local fields on the spectra is estimated to be small. The difference between the calculated and the experimental spectra of Se at lower energies is compared with the calculated local-field and continuum-exciton corrections for C, Si, and TlCl. The possible reasons for the differences in the ultraviolet region between the calculated one-electron spectra and the experimental ones of Se, Te, $ZrSe_2$, Si, Ge, GaP, GaAs, InAs, InSb, ZnS, and ZnSe are discussed.

## I. INTRODUCTION

The optical properties of trigonal Se have been investigated theoretically in the past with the pseudopotential (PSP) method by calculating the polarization-dependent Ehrenreich-Cohen[1-3] permittivity $\tilde{\epsilon} = \tilde{\epsilon}_1 + i\tilde{\epsilon}_2$ and the related optical spectra.[4-7] The most comprehensive study of these is empirical including the analysis of $\tilde{\epsilon}$ and the reflectivity up to $\sim 11$ eV.[4,5] The second empirical PSP (EPSP) study examines $\tilde{\epsilon}_2$ near the fundamental absorption edge.[6] The only self-consistent (SC) PSP study[7] presents the reflectivity up to $\sim 7$ eV, i.e., it essentially covers the energy range of the first main peak in the reflectivity. The PSP calculations utilize the pseudo-wave-functions which for Se even in the self-consistent pseudopotential case differ considerably from the true wave functions.[8] The measurement with the synchrotron radiation reveals sharp structure in the reflectivity up to $\sim 17$ eV.[9] In order to calculate the optical and electron-energy-loss spectra properly one must therefore calculate $\tilde{\epsilon}$ practically in the entire energy region where the transitions from the valence bands are important.

In the present study, the polarization-dependent $\tilde{\epsilon}$, reflectivity, absorption coefficient, and electron-energy-loss function are calculated in the energy range of $0-25$ eV using the SC non-muffin-tin Hartree-Fock-Slater energy-band results[10] and the momentum matrix elements rigorously evaluated with the true wave functions in the bulk of the first Brillouin zone (BZ).

An interesting problem in the case of semiconductors is the effect of the local fields on the optical and electron-energy-loss spectra.[11-16] In the case of Se contradictory results about the importance of the local-field effects have been reported.[6,7,17-19] Using the results of the present *ab initio* study we can test the validity of the model calculations which indicated large local fields[17-20] and indirectly gain insight into the local-field effects without actually calculating them. Finally, we discuss the possible reasons for the differences between the calculated one-electron spectra and the experimental ones found for several cubic and uniaxial semiconductors in the ultraviolet region.

## II. METHODS

The SC band-structure results (free from parametrization) have been obtained with 235 symmetry-adapted orthogonalized plane waves (OPW) at each of the eight symmetry points included in the calculation.[10] Slater's exchange-correlation potential is used.[21] Both the valence

and core states are included in the SC iteration. For the Ehrenreich-Cohen $\tilde{\epsilon}_2$ the eigenenergies and momentum matrix elements associated with the direct transitions are calculated at 131 symmetry-independent, regularly spaced $\vec{k}$ points in BZ using 201 OPW and the general (non-muffin-tin) SC crystal potential.[10] The formulas for the momentum matrix elements are presented in Appendix A.

The transition energies, their gradients, and the momentum matrix elements are calculated in a finer mesh (corresponding to 9216 cells in BZ) by using the quadratic Lagrangian interpolation scheme. The integration for $\tilde{\epsilon}_2$ is performed with the Gilat-Raubenheimer method.[22] A detailed description of the application of this approach is given elsewhere.[23]

In uniaxial Se the optical and electron-energy-loss spectra can be presented as parallel ($\|$) and perpendicular ($\perp$) components corresponding to the direction of the electric vector with respect to the trigonal $c$ axis. One can calculate $\epsilon_{1\|}$ and $\epsilon_{1\perp}$ from $\epsilon_{2\|}$ and $\epsilon_{2\perp}$, respectively, using the Kramers-Kronig integral relation. Further, the components of the reflectivity $R_\|$ and $R_\perp$, the absorption coefficient $K_\|$ and $K_\perp$, and the electron-energy-loss function $|\,\mathrm{Im}\epsilon_\|^{-1}\,|$ and $|\,\mathrm{Im}\epsilon_\perp^{-1}\,|$ can be calculated using the standard expressions.[24,25]

Thirty bands are taken into account in the calculation of $\tilde{\epsilon}_2$, which fully covers the energy range of $0-20$ eV. The diminishing of the calculated transitions above 20 eV has only a minute effect on the spectra in the analyzed energy range of $0-25$ eV because above 20 eV, $\tilde{\epsilon}_2$ is small. At lower energies the spectra are energetically too compressed, possibly due to the locality of Slater's exchange-correlation potential, whereas at higher energies the spectra are energetically too extended, possibly due to the different convergence rates of the distant bands.

The calculation was tested by checking the selection rules at the symmetry points in BZ, by calculating the momentum matrix elements in the star of the general $\vec{k}$ points, and by evaluating the effective numbers or the electrons from the sum rules[24-26] involving $\tilde{\epsilon}_2$, the absorption coefficient, and the electron-energy-loss function. It was found that the square of the momentum matrix element for the forbidden transitions was generally much smaller than that for the allowed transitions and typically between $10^{-8}$ and $10^{-4}$ in the Hartree atomic units. The rotational and time-reversal symmetry relations between the components of the momentum matrix elements were fulfilled typically with at least the relative accuracy of $10^{-4}$. The
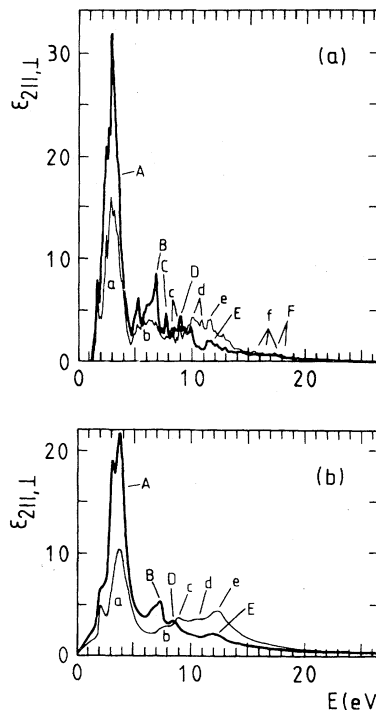


FIG. 1. Imaginary part of the permittivity $\tilde{\epsilon}_2$ of Se. (a) The SCOPW $\epsilon_{2\|}$ (thick line) and $\epsilon_{2\perp}$ (thin line). (b) The experimental $\epsilon_{2\|}$ (thick line) and $\epsilon_{2\perp}$ (thin line) from Ref. 9.

calculated effective numbers of the valence electrons per atom $n_{\mathrm{eff}}$, were 5.5 for $\epsilon_{2\|}$ and 5.4 for $\epsilon_{2\perp}$, $K_\|$, $K_\perp$, $|\,\mathrm{Im}\epsilon_\|^{-1}\,|$, and $|\,\mathrm{Im}\epsilon_\perp^{-1}\,|$, which displays excellent mutual consistency. These values of $n_{\mathrm{eff}}$ are quite near six which is the number of the outer atomic $s$ and $p$ electrons occupying the valence states in the crystal. [At high energies $n_{\mathrm{eff}}$ should saturate at only slightly above six because the oscillator strengths coupling the core and valence states are probably small owing to the large energy separations of the states ($\gtrsim 40$ eV).[10,27]] The calculated $n_{\mathrm{eff}}$ for $\epsilon_{2\|}$ and $\epsilon_{2\perp}$ reached four at 11.5 and 13.0 eV, respectively. These energies agree well with the results of Nielsen et al.[28] whose calculations, based on the empirical $\tilde{\epsilon}_2$ data of Leiga[29] and Bammes et al.[9] gave $n_{\mathrm{eff}}=4$ at $12-14$ eV.

## III. RESULTS AND DISCUSSION

The calculated $\tilde{\epsilon}_2$ is presented in Fig. 1(a) and $\tilde{\epsilon}_2$ derived from the measured reflectivity at 300 K (Ref. 9) is shown in Fig. 1(b) for comparison. The calculated $\tilde{\epsilon}_2$ is in good agreement with the experimental ones.[9,29-31] The extrapolation of the measured reflectivity below 3 eV may be responsible
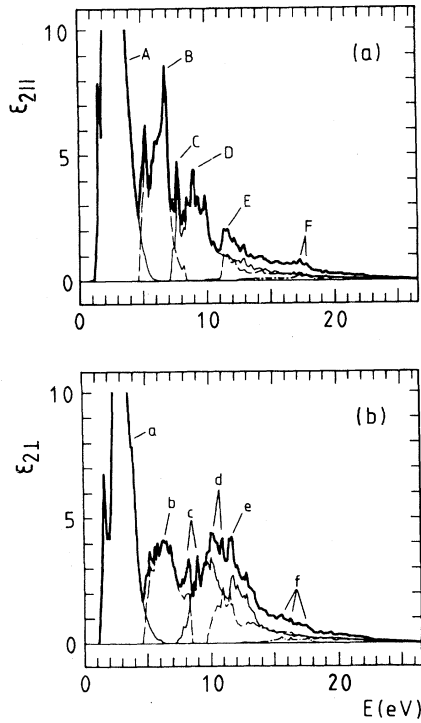
FIG. 2. Triplet decomposition of the SCOPW $\epsilon_{2||}$ and $\epsilon_{2\perp}$ of Se [(a) and (b), respectively]. The solid thick line corresponds to the total $\tilde{\epsilon}_2$. The solid, dashed, and dash-dotted thin lines represent the contributions to $\tilde{\epsilon}_2$ from the $p$ lone-pair VB3, $p$ bonding VB2, and $s$ bonding VB1, respectively.

for the disappearing of the optical gap in the experimental $\tilde{\epsilon}_2$ [Fig. 1(b)]. The theoretical $\tilde{\epsilon}_2$ is higher than the experimental $\tilde{\epsilon}_2$ below $\sim 11$ eV and mainly lower above $\sim 11$ eV (Fig. 1). We compare the calculated peak positions with the experimental ones[9,30] in Table I and find close agreement. The cusp at 5.3 eV and peak $C$ found in the calculated $\epsilon_{2||}$ may have been absorbed in the experimental $\epsilon_{2||}$ by a close prominent peak, the former by peak $A$ and the latter by peak $B$ (the experimental peak $B$ in Ref. 29 reveals a shoulder at high-energy flank possibly corresponding to the calculated peak $C$).

In Se the nine valence bands and the three lowest conduction bands are grouped into four energetically separated triplets.[10,32] $\epsilon_{2||}$ and $\epsilon_{2\perp}$ are decomposed according to the initial triplets involved in the transitions in Fig. 2. The valence-band triplets are labeled with VB1, VB2, and VB3 (placed according to increasing energy) corresponding to the $s$ bonding, $p$ bonding, and $p$ lone-pair triplets, respectively.[8,10,32] The lowest $p$ antibonding conduction-band triplet is labeled with CB1. CB2 denotes the higher conduction bands of which
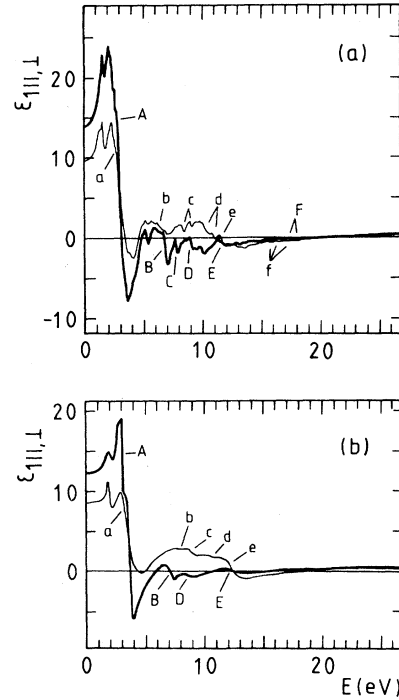
FIG. 3. Real part of the permittivity $\tilde{\epsilon}_1$ of Se. (a) The SCOPW $\epsilon_{1||}$ (thick line) and $\epsilon_{1\perp}$ (thin line). (b) The experimental $\epsilon_{1||}$ (thick line) and $\epsilon_{1\perp}$ (thin line) from Ref. 9.

the lowest ones are mainly of $d$-$s$ type. In Fig. 2 the gaps in the VB3 contribution (solid thin lines) at $\sim 7$ eV and in the VB2 contribution (dashed thin lines) at $\sim 9$ eV are caused by the gap between CB1 and CB2. The origin of the peaks is presented in Table I. We see from Fig. 2 and Table I that the transitions from VB3 dominate $\tilde{\epsilon}_2$ ($\epsilon_{2\perp}$ in particular), and that those from VB2 cause large peaks $(B,E)$ only in $\epsilon_{2||}$. Transitions VB1$\rightarrow$CB2 have practically no effect on $\tilde{\epsilon}_2$. Transitions VB3$\rightarrow$CB2 are the primary cause for the crossing of the calculated $\epsilon_{2||}$ and $\epsilon_{2\perp}$ at 9.5 eV close to that of the experimental $\epsilon_{2||}$ and $\epsilon_{2\perp}$ (Ref. 9) at $\sim 9$ eV.

Below 4.5, 4.5$-$8, 8$-$15, 15$-$18, and above 18 eV the anisotropy is mainly due to transitions VB3$\rightarrow$CB1, VB2$\rightarrow$CB1, VB3 and VB2$\rightarrow$CB2, VB1$\rightarrow$CB1, and VB2$\rightarrow$CB2, respectively (Fig. 2 and Table I).

The calculated $\tilde{\epsilon}_1$ is presented in Fig. 3(a) and $\tilde{\epsilon}_1$ derived from the measured reflectivity at 300 K (Ref. 9) is shown in Fig. 3(b) for comparison. The descending slopes associated with the preceding peaks or shoulders in $\tilde{\epsilon}_1$ are labeled according to the peaks in $\tilde{\epsilon}_2$ (Fig. 1) and their origin can be understood with the aid of Fig. 2 and Table I. The theoretical $\tilde{\epsilon}_1$ is in good agreement with the experi-

TABLE I. The position and origin of the main peaks in $\tilde{\epsilon}_2$, the reflectivity, and the absorption coefficient of Se. The transitions causing an appreciable background are put into parentheses. All numbers are given in eV.

| | Peak | $\tilde{\epsilon}_2$ Theory[a] | Expt.[b] | Reflectivity Theory[a] | Expt.[b] | Absorption coefficient Theory[a] | Expt.[c] | Origin |
|---|---|---|---|---|---|---|---|---|
| ‖ | A | 3.0 | 3.5 | 3.7 | 3.9 | 3.6 | 3.9 | VB3→CB1 |
| | B | 6.8 | 7.3 | 7.1 | 7.5 | 6.9 | 7.6 | VB2→CB1 |
| | C | 7.8 | | 8.0 | | | | VB3→CB2 |
| | D | 9.0 | 8.5 | 10.2 | 9.1 | 10.0 | 9.6 | VB3→CB2 |
| | E | 11.6 | 12.0 | 13.2 | 13.0 | 11.7 | 12.2 | VB2→CB2, (VB3→CB2) |
| | F | 17.6 | | 17.9 | 16.2 | 17.6 | | VB1→CB1, (VB3 and VB2→CB2) |
| ⊥ | a | 2.9 | 3.5 | 3.5 | 3.9 | 3.6 | 3.9 | VB3→CB1 |
| | b | 6.2 | 7.5 | 6.9 | 7.4 | 6.9 | 7.5 | VB2→CB1 |
| | c | 8.6 | 8.9 | 8.6 | 8.9 | 8.7 | 9.1 | VB2→CB1, VB3→CB2 |
| | d | 10.5 | 10.6 | 10.6 | 10.5 | 10.7 | 10.6 | VB3 and VB2→CB2 |
| | e | 11.6 | 12.3 | 13.6 | 13.5 | 11.7 | 13.6 | VB3→CB2, (VB2→CB2) |
| | f | 16.5 | | 16.7 | 16.4 | 16.5 | | VB1→CB1, (VB3 and VB2→CB2) |

[a]Present study.
[b]Peaks A and a from Ref. 30, others from Ref. 9.
[c]Peaks A and a from Ref. 30, others from Ref. 29.

mental $\tilde{\epsilon}_1$.[9,29,30] The calculated peaks A and a are higher than the corresponding experimental peaks and after peaks A and a the calculated $\tilde{\epsilon}_1$ is mainly smaller than the experimental $\tilde{\epsilon}_1$ (this behavior is particularly distinct for $\epsilon_{1\parallel}$).

In Table II the theoretical optical refractive index $n_{\parallel,\perp}=\epsilon_{1\parallel,\perp}^{1/2}$ (calculated at 0 eV) is compared with the experimental ones[33-36] obtained in the middle or near infrared region. The theoretical refractive index is somewhat larger than the experimental ones. The contribution of the transitions from the valence-band triplets to $n_{\parallel}$ and $n_{\perp}$ is also shown in Table II. The transitions from VB3 are the main constituents of the refractive index and

mainly cause its anisotropy (Table II).

$\epsilon_{1\parallel}$ and $\epsilon_{1\perp}$ cross at 11.7 eV and they cross zero for the last time at 19.1 and 19.7, respectively [Fig. 3(a)]. In Se the plasma peak appears near the last zero of $\tilde{\epsilon}_1$ (see below).

The theoretical reflectivity is shown in Fig. 4(a) and the reflectivity measured with the synchrotron radiation at 300 K (Ref. 9) is presented in Fig. 4(b) for comparison. The peaks in the reflectivity are labeled similarly as the peaks in $\tilde{\epsilon}_2$ (Fig. 1) and their origin as well as their calculated and measured positions are presented in Table I (see also Fig. 2). The calculated and the measured reflectivities are in close agreement (Fig. 4 and Table I).

TABLE II. The optical refractive index $n_{\parallel,\perp}=\epsilon_{1\parallel,\perp}^{1/2}$ of Se. The theoretical values are obtained at 0 eV and the experimental ones in the middle or near infrared region. The last three columns show the SCOPW $n_{\parallel}$ and $n_{\perp}$ obtained by taking into account the transitions from one valence-band triplet at a time.

| | Experiments | | | | Theory | | | Contributing triplets VB1 | VB2 | VB3 |
|---|---|---|---|---|---|---|---|---|---|---|
| $n_{\parallel}$ | 3.58[a] | 3.24[b] | 3.65[c] | 3.2[d] | 3.75[e] | 3.5[f] | 3.6[g] | 1.02 | 1.58 | 3.54 |
| $n_{\perp}$ | 2.78[a] | 2.60[b] | 2.87[c] | 2.5[d] | 3.13[e] | 2.6[f] | 2.4[g] | 1.01 | 1.54 | 2.89 |

[a]Reference 33.
[b]Reference 34.
[c]Reference 35.
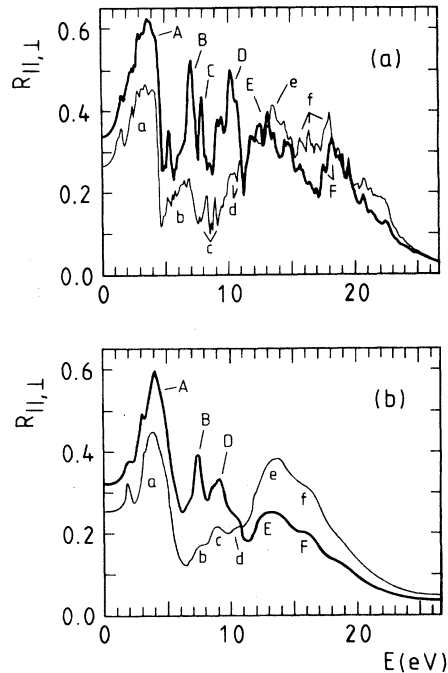[d]Reference 36.
[e]Present study.
[f]Reference 17.
[g]Reference 19.

FIG. 4. Reflectivity $R_\parallel$, $R_\perp$ of Se. (a) The SCOPW $R_\parallel$ (thick line) and $R_\perp$ (thin line). (b) The measured $R_\parallel$ (thick line) and $R_\perp$ (thin line) from Ref. 9.
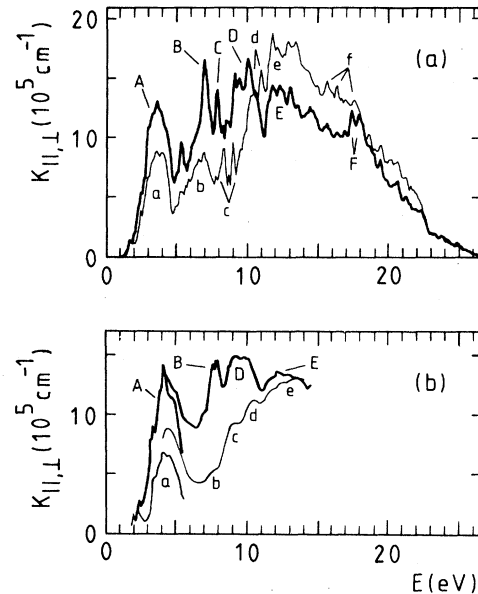


FIG. 5. Absorption coefficient $K_\parallel$, $K_\perp$ of Se. (a) The SCOPW $K_\parallel$ (thick line) and $K_\perp$ (thin line). (b) The experimental $K_\parallel$ (thick line) and $K_\perp$ (thin line) from Ref. 30 (ending at $\sim 5.5$ eV) and from Ref. 29 (starting at $\sim 4$ eV).

Not only are the experimental salient features well reproduced in the theoretical reflectivity but also the peak heights, shapes, and positions are in good accordance with the measured ones.[9,17,29,30,37−41] The theoretical peaks $D$ and $d$ agree more closely with the corresponding experimental ones in Refs. 29 and 41 than with those in Fig. 4(b).[9] The measured $R_\perp$ around 12 eV in Refs. 29 and 41 is low and does not increase as the calculated and measured[9] $R_\perp$ in Fig. 4. Above $\sim 7$ eV the calculated $R_\parallel$ is higher than the measured $R_\parallel$ and similar difference can be found in $R_\perp$ above $\sim 17$ eV (Fig. 4). This difference is due to the fact that the calculated $\tilde{\epsilon}_1$ and $\tilde{\epsilon}_2$ are smaller than the experimental $\tilde{\epsilon}_1$ and $\tilde{\epsilon}_2$, respectively (see above). It may be possible that the measured reflectivity has been obscured by surface contamination and/or damage (see below).

Below 5, 5−8.5, 8.5−15, 15−19, and above 19 eV the anisotropy is mainly due to transitions VB3→CB1, VB2→CB1, VB3 and VB2→CB2, VB1→CB1, and VB2→CB2, respectively (Table I and Fig. 2). In the energy range of 8.5−15 eV transitions VB3→CB2 contribute to $R_\parallel$ (peak $D$) at lower energies than to $R_\perp$ (peak $d$-$e$) causing the anisotropy at the low-energy flank of the range whereas transitions VB2→CB2 cause the anisotro-

py at the high-energy one.[42]

The calculated absorption coefficient is presented in Fig. 5(a) and those derived from the measured reflectivity at 300 K (Ref. 29) and at 20 K (Ref. 30) are shown in Fig. 5(b) for comparison. We are not aware of any experimental absorption coefficient associated with the valence-band transitions above 14.4 eV. The peaks in the absorption coefficient are labeled similarly as the peaks in $\tilde{\epsilon}_2$ (Fig. 1) and their origin as well as their calculated and experimental positions are presented in Table I (see also Fig. 2). The theoretical absorption coefficient is in good agreement with the experimental ones (Fig. 5). The experimental peak $B$ [Fig. 5(b)] appears distinctly twofold, the high-energy part possibly corresponding to the calculated peak $C$ [Fig. 5(a)]. The calculated $K_\perp$ around 12 eV is higher than the experimental $K_\perp$ by a factor of $\sim 1.5$ (Fig. 5). [At higher energies $K_\perp$ should be higher than $K_\parallel$ because the sum rule requires that the areas surrounded by $K_\parallel$ or $K_\perp$ and the energy axis are the same[25,26] (the areas for the calculated $K_\parallel$ and $K_\perp$ are the same, see Sec. II).] The anisotropy regions in the absorption coefficient are the same as those in $\tilde{\epsilon}_2$ (see above).

We present the calculated and the measured[9] electron-energy-loss functions in Figs. 6(a) and 6(b), respectively. The calculated and the measured
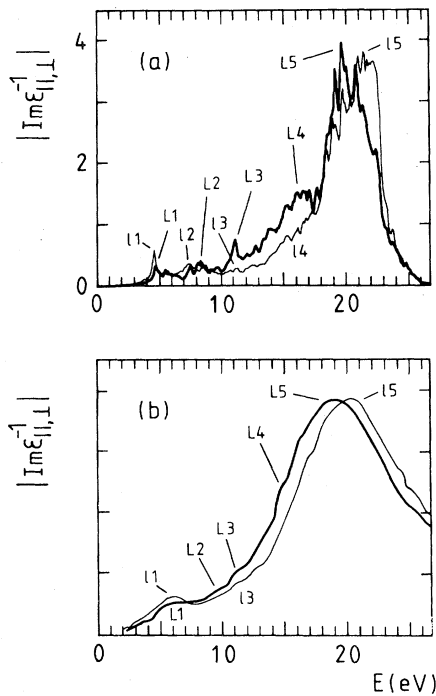
FIG. 6. Electron-energy-loss function $|\mathrm{Im}\epsilon_{||}^{-1}|$, $|\mathrm{Im}\epsilon_{\perp}^{-1}|$ of Se. (a) The SCOPW $|\mathrm{Im}\epsilon_{||}^{-1}|$ (thick line) and $|\mathrm{Im}\epsilon_{\perp}^{-1}|$ (thin line). (b) The measured $|\mathrm{Im}\epsilon_{||}^{-1}|$ (thick line) and $|\mathrm{Im}\epsilon_{\perp}^{-1}|$ (thin line) from Ref. 9 (arbitrary units).

electron-energy-loss functions are in good accordance although the salient features appear in the energy region where $\overline{\epsilon}$ is small and sensitive to inaccuracies. The calculated peak positions [(in eV) 4.7 ($L1$), 8.4 ($L2$), 11.1 ($L3$), $\sim16$ ($L4$), $\sim19.6$ ($L5$), 4.6 ($l1$), 7.3 ($l2$), 11.1 ($l3$), $\sim16$ ($l4$), and 20.9 ($l5$)] agree well with those measured by Bammes et al.[9] [(in eV) 6 ($L1$), 9 ($L2$), 11 ($L3$), 14.5 ($L4$) 19.0 ($L5$), 6 ($l1$), 11 ($l3$), 20.3 ($l5$)]. Coincident values of 6.9, 12.1, and 19.0 eV (Ref. 43) and $-$, 10, and 19.9 eV (Ref. 27) were experimentally obtained for the average positions of peaks $L1$ and $l1$, $L3$ and $l3$, and $L5$ and $l5$, respectively, for crystalline films. The transitions below the plasma region force the calculated and measured single plasma peaks $L5$ and $l5$ to appear at somewhat higher energies than the free-electron plasma frequency of 17.4 eV of the six $s$ and $p$ electrons of the Se atom.[44]

The calculated peak positions are in good agreement also with those in the electron-energy-loss function derived from the measured reflectivity.[9,29] However, the calculated electron-energy-loss function is much higher than the derived ones. The calculated plasma peaks $L5$ and $l5$ in particular are

higher than the derived ones[9] by a factor of $\sim2.5$. We associate this disagreement with the intensity difference in $\overline{\epsilon}$ and the reflectivity between the calculation and measurement at high energies (see below).

The anisotropy below 8, 8$-$15, 15$-$18, and above 18 eV is due to transitions VB2$\rightarrow$CB1, VB3 and VB2$\rightarrow$CB2, VB1$\rightarrow$CB1, and VB2$\rightarrow$CB2, respectively (cf. Fig. 2).

Of the previous studies of Se the EPSP study by Sandrock analyzes[4,5] $\overline{\epsilon}$ and the reflectivity in terms of the transitions between the bands. The present self-consistent orthogonalized-plane-wave (SCOPW) results contradict the EPSP results in a few important respects. Peaks $B$ and $D$ in the SCOPW $\epsilon_{2||}$ are due to transitions VB2$\rightarrow$CB1 and VB3$\rightarrow$CB2, respectively, whereas the EPSP $\epsilon_{2||}$ indicates the reverse order for these transitions. In the SCOPW $\epsilon_{2\perp}$ transitions VB2$\rightarrow$CB1 mainly contribute below 8.5 eV whereas in the EPSP study these transitions contribute a large background to $\epsilon_{2\perp}$ up to $\sim12$ eV. According to the SCOPW study the crossing of $\epsilon_{2||}$ and $\epsilon_{2\perp}$ is mainly due to transitions VB3$\rightarrow$CB2 whereas in the EPSP study the crossing is mainly due to transitions VB2$\rightarrow$CB1.

In the experimental $\epsilon_2$ of amorphous Se a broad peak is found between 3 and 5 eV and between 7 and 9 eV.[31,45] The decomposition of the SCOPW $\overline{\epsilon}_2$ of trigonal Se (Fig. 2 and Table I) supports the interpretation that the first peak of $\epsilon_2$ of amorphous Se may be due to transitions VB3$\rightarrow$CB1 and the second peak due to transitions VB2$\rightarrow$CB1 and VB3$\rightarrow$CB2. The SCOPW interpretation disagrees partially with those given in Ref. 46 (where it was suggested that the second peak was fully due to transitions VB2$\rightarrow$CB1) and in Ref. 47 (where it was found that transitions VB1 and VB2 and VB3$\rightarrow$CB1 contribute to both peaks).

The large increase of the measured reflectivity of Se under pressure was interpreted to indicate that the local-field effects are large.[17] The calculation of the refractive index ($n_{||}$ and $n_{\perp}$) of trigonal Se yielded the same conclusion.[18,19] Both investigations were based on the permittivity models from which $n_{||}$ and $n_{\perp}$ could be calculated. In Table II the SCOPW $n_{||}$ and $n_{\perp}$ (no local fields) are compared with those of the model calculations[17,19] (local fields included) and the experiments[33$-$36] for trigonal Se. It is found that rather good agreement with the experiments has been theoretically obtained both with and without the local-field effects. It is not known how well the spectra of the model calculations[17,19] would agree with the experiments

above 0 eV. All the SCOPW spectra agree well with the experimental ones in the wide energy range of 0—25 eV, which inevitably supports the conclusion that the local-field effects in Se should be much smaller than predicted on the basis of the model studies.[17,19] This conclusion agrees with those of the recent investigations where it was found that the increased interchain interactions, and not the local fields, are the most important factor causing the pressure-induced increase in the reflectivity.[6,7,48]

It was recently found for C (Ref. 13), Si (Ref. 14), and TlCl (Ref. 15) that the local-field and continuum-exciton corrections improved agreement with experiments considerably by shifting the optical spectra to the low-energy side and by increasing the first (low-energy) peak of $\epsilon_2$. It is interesting to notice that to improve the agreement between the SCOPW and experimental spectra of Se the corrections needed should be opposite to those calculated for C (Ref. 13), Si (Ref. 14), and TlCl.[15] The SCOPW $\epsilon_2$ is larger than the experimental $\epsilon_2$ at lower energies and the calculated first peak of $\epsilon_2$ ($A$ or $a$) in particular is higher than the corresponding experimental peak (Fig. 1). The local-field and continuum-exciton corrections for Si (Ref. 14) and TlCl (Ref. 15) increased the refractive index improving agreement with experiments whereas for Se the SCOPW $n_{\parallel}$ and $n_{\perp}$ are already somewhat larger than the experimental ones (Table II). Our result for Se is similar to those found for Te (Refs. 49 and 50), ZrS$_2$ (Refs. 51 and 52), and ZrSe$_2$.[52]

We found above that in the ultraviolet region the calculated reflectivity and electron-energy-loss function were higher than the measured reflectivity and the associated derived electron-energy-loss function, respectively. Similar differences have been found by Louie et al.[12] in the EPSP study for Si, Sturm[16] in the EPSP study for Si, Ge, GaP, GaAs, InAs, and InSb, Wang and Klein[53] in the ab initio self-consistent linear combination of Gaussian orbitals (SCLCGO) study for Si, Ge, GaP, GaAs, ZnS, and ZnSe, and Isomäki and von Boehm in the ab initio SCOPW study for Te (Ref. 50) and ZrSe$_2$.[52] An apparent obscurity in the comparison between the calculations and the experiments is caused by the fact that the measured primary plasma peaks (obtained directly from the electron-energy-loss measurements) for Si, Ge (Ref. 54), GaP, GaAs, InAs, and InSb (Ref. 55) are higher by a factor of $\sim$3 or more than those derived from the measured reflectivities. This

disagreement between different experiments may be due to surface contamination and/or damage, which are known to reduce the intensity (and possibly also to wipe out salient features) of the measured reflectivities and the associated derived electron-energy-loss functions of Si, Ge, GaP, GaAs, InAs, and InSb.[54–64] Therefore, the measured primary electron-energy-loss data should be preferred at high energies.[24] The heights of the plasma peaks calculated by Wang and Klein[53] in the ab initio SCLCGO study for Si, Ge, GaP, and GaAs are already without local-field corrections in rather close agreement with the primary measured ones.[54,55] In fact, the calculated large lowering EPSP local-field corrections for Si (Refs. 12 and 16), Ge, and GaAs (Ref. 16) would considerably worsen this agreement. (Hanke and Sham[14] noted, however, that the calculated continuum-exciton corrections would again enhance the plasma peak of Si.) We found that the calculated electron-energy-loss function (without local fields) of Se as well as those of Te (Ref. 50) and ZrSe$_2$ (Ref. 52) agrees closely with the measured primary one. This agreement seems to indicate that the local-field effects are small. Hence the difference between the calculated spectra and the measured reflectivity and associated derived spectra in the ultraviolet region seems to be mainly due to the sensitivity of the measured reflectivity to surface quality.

## IV. CONCLUSIONS

In this study the optical and electron-energy-loss spectra of trigonal Se are calculated using the self-consistent non-muffin-tin Hartree-Fock-Slater energy-band results and the momentum matrix elements which are rigorously evaluated in the bulk of the first Brillouin zone. The analysis is extended to the energy range of 0—25 eV where the transitions from the valence bands are important. The theoretical results agree closely with the experiments.

The parallel optical spectra are formed of the four main peaks $A$, $B$, $D$, and $E$ mainly due to transitions VB3→CB1, VB2→CB1, VB3→CB2, and VB3 and VB2→CB2, respectively. The perpendicular optical spectra are formed of the two main peaks $a$ and $d$-$e$ mainly due to transitions VB3→CB1 and VB3 and VB2→CB2, respectively. Transitions VB1→CB1 cause peaks ($F$ and $f$) at high energies. The most significant contribution to the spectra comes from the transitions from VB3 which dominate the perpendicular spectra in par-

ticular. The transitions from VB2 yield the conspicuous features (peaks $B$ and $E$) only in the parallel optical spectra. Transitions VB1→CB2 have an insignificant contribution to the spectra. Transitions VB3→CB2 are the primary cause for the crossing of the optical curves with different polarizations around 10 eV.

The results for trigonal Se are also used to interpret the origin of the two peaks in $\epsilon_2$ of amorphous Se: the first (lower-energy) peak is found to be due to transitions VB3→CB1 and the second peak due to both transitions VB2→CB1 and VB3→CB2.

On the basis of the present results it is concluded that the local-field effects in Se should be much smaller than those predicted in the recent studies.[17,19] We found that to get even closer agreement with the experiments at lower energies the corrections needed for the calculated *ab initio* spectra of Se should be opposite to the calculated local-field and continuum-exciton corrections for C (Ref. 13), Si (Ref. 14), and TlCl.[15] The disagreement in the ultraviolet region between the calculated and measured reflectivity and between the calculated and derived electron-energy-loss function of Se [and possibly the similar disagreement found for Te (Ref. 50), ZrSe$_2$ (Ref. 52), Si (Refs. 12, 16, and 53), Ge, GaP, GaAs, (Refs. 16 and 53), InAs, InSb (Ref. 16), ZnS, and ZnSe (Ref. 53)] may be mainly due to the sensitivity of the measured reflectivity to the quality of the crystal surface.

## APPENDIX A: THE MOMENTUM MATRIX ELEMENTS

The momentum matrix elements used in the PSP calculation with OPW for the special case of Na are given in Ref. 65. The formulas for the SCOPW calculation to be presented in this appendix are fully general. The momentum matrix elements are calculated between the wave functions expanded as a linear combination of OPW $X_{\vec{k}_i}$ $(\vec{k}_i = \vec{k} + \vec{G}_i$ where $\vec{k}$ is a reduced-wave vector and $\vec{G}_i$ a reciprocal-lattice vector). A lengthy calculation gives the following result for the momentum matrix elements between OPW in the Hartree atomic units:

$$\langle X_{\vec{k}_i} \mid \vec{p} \mid X_{\vec{k}_j} \rangle = \vec{k}_i \delta_{\vec{G}_i \vec{G}_j} - (\vec{k}_i + \vec{k}_j) \frac{4\pi}{\Omega_0} \sum_q e^{i(\vec{G}_j - \vec{G}_i)\cdot\vec{\tau}_q} \sum_l (2l+1) P_l(\cos\beta_{\vec{k}_i \vec{k}_j}) \sum_n b^q_{nlk_i} b^q_{nlk_j}$$

$$+ \frac{16\pi^2}{\Omega_0} \sum_q e^{i(\vec{G}_j - \vec{G}_i)\cdot\vec{\tau}_q} \sum_l \sum_{l'} (-i)^{l+1} i^{l'} \sum_n \sum_{n'} b^q_{nlk_i} b^q_{n'l'k_j} (E^q_{n'l'} - E^q_{nl}) \int_0^\infty R^q_{nl}(r) R^q_{n'l'}(r) r^3 dr$$

$$\times \sum_m \sum_{m'} Y^l_m(\theta_{\vec{k}_i}, \phi_{\vec{k}_i}) Y^{l'}_{m'}(\theta_{\vec{k}_j}, \phi_{\vec{k}_j})^* \langle l,m \mid \vec{u}_r \mid l',m' \rangle \ .$$

$$(A1)$$

In Eq. (A1) $q$ labels the atoms in the primitive unit cell, $\vec{\tau}_q$ is the position vector of the atom $q$, $\Omega_0$ is the volume of the primitive unit cell, $n$, $l$, $m$, and $n'$, $l'$, $m'$ are the principal, azimuthal, and magnetic quantum numbers for the core states, respectively, $R^q_{nl}$ is the radial part of the core function of the atom $q$, and $E^q_{nl}$ the corresponding eigenenergy, $P_l$ is the Legendre polynomial, $\beta_{\vec{k}_i \vec{k}_j}$ is the angle between $\vec{k}_i$ and $\vec{k}_j$, $Y^l_m$ is the spherical harmonic with the Condon-Shortley phase, $r,\theta,\phi$ are the spherical polar coordinates, $\vec{u}_r$ is the unit vector associated with $r$, and $b^q_{nlk}$ is the radial orthogonalization coefficient

$$b^q_{nlk} = \int_0^\infty R^q_{nl}(r) j_l(kr) r^2 dr \ , \tag{A2}$$

where $j_l$ is the spherical Bessel function. The matrix elements of $\vec{u}_r$ between $Y^l_m$ $\langle l,m \mid \vec{u}_r \mid l',m' \rangle$ can be calculated exactly and the result is[66]

$$\langle l,m \mid \vec{u}_r \mid l+1, m+1 \rangle = -f(l+1,m+1)(\vec{u}_x + i\vec{u}_y) \ , \tag{A3}$$

$$\langle l,m \mid \vec{u}_r \mid l+1, m \rangle = g(l+1,m)\vec{u}_z \ , \tag{A4}$$

$$\langle l,m \mid \vec{u}_r \mid l+1,m-1 \rangle = f(l+1,-(m-1))(\vec{u}_x - i\vec{u}_y) , \qquad (A5)$$

$$\langle l,m \mid \vec{u}_r \mid l-1,m+1 \rangle = f(l,-m)(\vec{u}_x + i\vec{u}_y) , \qquad (A6)$$

$$\langle l,m \mid \vec{u}_r \mid l-1,m \rangle = g(l,m)\vec{u}_z , \qquad (A7)$$

$$\langle l,m \mid \vec{u}_r \mid l-1,m-1 \rangle = -f(l,m)(\vec{u}_x - i\vec{u}_y) , \qquad (A8)$$

where $\vec{u}_x$, $\vec{u}_y$, and $\vec{u}_z$ are the Cartesian unit vectors and

$$f(l,m) = \frac{1}{2} \left[ \frac{(l+m-1)(l+m)}{(2l-1)(2l+1)} \right]^{1/2} , \qquad (A9)$$

$$g(l,m) = \left[ \frac{(l-m)(l+m)}{(2l-1)(2l+1)} \right]^{1/2} . \qquad (A10)$$

Other $\langle l,m \mid \vec{u}_r \mid l',m' \rangle$ are zero. The calculation of the momentum matrix elements [obtained with the aid of the OPW expansion coefficients and Eq. (A1)] can be confined to the irreducible wedge of BZ ($\frac{1}{12}$ of BZ for Se) using the rotational (and time-reversal) symmetry relations.

[1]H. Ehrenreich and M. H. Cohen, Phys. Rev. 115, 786 (1959).

[2]S. L. Adler, Phys. Rev. 126, 413 (1962).

[3]N. Wiser, Phys. Rev. 129, 62 (1963).

[4]R. Sandrock, Phys. Rev. 169, 642 (1968).

[5]R. Sandrock, Phys. Status Solidi B 43, 199 (1971).

[6]H. Wendel, R. M. Martin, and D. J. Chadi, Phys. Rev. Lett. 38, 656 (1977).

[7]J. D. Joannopoulos, T. Starkloff, and M. Kastner, Phys. Rev. Lett. 38, 660 (1977).

[8]H. Isomäki and J. von Boehm, J. Phys. C 13, L485 (1980).

[9]P. Bammes, R. Klucker, E. E. Koch, and T. Tuomi, Phys. Status Solidi B 49, 561 (1972).

[10]J. von Boehm and H. Isomäki, J. Phys. C 13, 4953 (1980).

[11]A. Baldereschi, J. Phys. Soc. Jpn. 49, A155 (1980).

[12]S. G. Louie, J. R. Chelikowsky, and M. L. Cohen, Phys. Rev. Lett. 12, 4501 (1975).

[13]W. Hanke and L. J. Sham, Phys. Rev. B 12, 4501 (1975).

[14]W. Hanke and L. J. Sham, Phys. Rev. B 21, 4656 (1980).

[15]W. Schäfer and M. Schreiber, Solid State Commun. 38, 1241 (1981).

[16]K. Sturm, Phys. Rev. Lett. 40, 1599 (1978).

[17]M. Kastner and R. R. Forberg, Phys. Rev. Lett. 36, 740 (1976).

[18]F. Nizzoli, J. Phys. C 11, 673 (1978).

[19]F. Nizzoli, in The Physics of Selenium and Tellurium, edited by E. Gerlach and P. Grosse (Springer, Berlin, 1979), p. 31.

[20]F. Nizzoli, Nuovo Cimeno 39B, 135 (1977).

[21]J. C. Slater, Phys. Rev. 81, 385 (1951).

[22]G. Gilat and L. J. Raubenheimer, Phys. Rev. 144, 390 (1966).

[23]J. von Boehm and H. Isomäki, J. Phys. C 13, 3181 (1980).

[24]D. L. Greenaway and G. Harbeke, Optical Properties and Band Structure of Semiconductors (Pergamon, Oxford, 1968).

[25]F. Bassani and G. Pastori Parravicini, Electronic States and Optical Transitions in Solids (Pergamon, Oxford, 1975).

[26]D. Y. Smith and E. Shiles, Phys. Rev. B 17, 4689 (1978).

[27]N. J. Shevchik, M. Cardona, and J. Tejeda, Phys. Rev. B 8, 2833 (1973).

[28]P. Nielsen, M. Slade, and R. Zallen (unpublished), quoted by P. Nielsen, Phys. Rev. B 10, 1673 (1974).

[29]A. G. Leiga, J. Opt. Soc. Am. 58, 880 (1968).

[30]S. Tutihasi and I. Chen, Phys. Rev. 158, 623 (1967).

[31]J. Stuke, J. Non-Cryst. Solids 4, 1 (1970).

[32]T. Starkloff and J. D. Joannopoulos, J. Chem. Phys. 68, 579 (1978).

[33]R. S. Caldwell and H. Y. Fan, Phys. Rev. 114, 664 (1959).

[34]V. Prosser, Czech. J. Phys. B 10, 306 (1960).

[35]H. Gobrecht and A. Tausend, Z. Phys. 161, 205 (1961).

[36]F. Eckart and W. Henrion, Phys. Status Solidi 2, 841 (1962).

[37]J. Stuke and H. Keller, Phys. Status Solidi 7, 189 (1964).

[38]W. Henrion, Phys. Status Solidi 20, K145 (1967).

[39]W. Henrion, Phys. Status Solidi 22, K33 (1967).

[40]E. Mohler, J. Stuke, and G. Zimmerer, Phys. Status Solidi 22, K49 (1967).

[41]A. G. Leiga, J. Appl. Phys. 39, 2149 (1968).

[42]H. M. Isomäki and J. von Boehm, Solid State Commun. 41, 765 (1982).

[43]H. Friedmann, Z. Naturforsch. Teil A 11, 373 (1956).

[44]D. Pines, Rev. Mod. Phys. 28, 184 (1956).

[45]A. G. Leiga, J. Opt. Soc. Am. 58, 1441 (1968).

[46]M. Kastner, Phys. Rev. Lett. 28, 355 (1972).

[47]I. Chen, Phys. Rev. B 7, 3672 (1973).

[48]H. M. Isomäki and J. von Boehm (unpublished).

[49]T. Starkloff and J. D. Joannopoulos, Phys. Rev. B 19,

1077 (1979).

[50]H. M. Isomäki, J. von Boehm, and T. Stubb, Phys. Rev. B (in press).

[51]H. M. Isomäki and J. von Boehm, J. Phys. C 14, L1043 (1981).

[52]H. M. Isomäki and J. von Boehm, Phys. Rev. B (in press).

[53]C. S. Wang and B. M. Klein, Phys. Rev. B 24, 3417 (1981).

[54]K. Zeppenfeld and H. Raether, Z. Phys. 193, 471 (1966).

[55]C. von Festenberg, Z. Phys. 227, 453 (1969).

[56]H. Raether, in Springer Tracts in Modern Physics, edited by G. Höhler (Springer, Berlin, 1965), Vol. 38.

[57]L. Marton and J. Toots, Phys. Rev. 160, 602 (1967).

[58]H. Raether, Helv. Phys. Acta 41, 1112 (1968).

[59]J. Daniels, C. von Festenberg, H. Raether, and K. Zeppenfeld, in Springer Tracts in Modern Physics, edited by G. Höhler (Spinger, Berlin, 1970), Vol. 54.

[60]T. M. Donovan, W. E. Spicer, J. M. Bennett, and E. J. Ashley, Phys. Rev. B 2, 397 (1970).

[61]H. R. Philipp, J. Appl. Phys. 43, 2835 (1972).

[62]A. E. Morgan, Surf. Sci. 43, 150 (1974).

[63]P. J. Zanzucchí and M. T. Duffy, Appl. Opt. 17, 3477 (1978).

[64]J. Stiebling, Z. Phys. B 31, 355 (1978).

[65]J. A. Appelbaum, Phys. Rev. 144, 435 (1966).

[66]V. A. Fock, Fundamentals of Quantum Mechanics (Mir, Moscow, 1978).